Chemosphere 247 (2020) 125902

Contents lists available at ScienceDirect

Chemosphere

journal homepage: www.elsevier.com/locate/chemosphere

Iron mineral-humic acid complex enhanced Cr(VI) reduction by *Shewanella oneidensis* MR-1

Abdelkader Mohamed [a, b], Lu Yu [a], Yu Fang [a], Noha Ashry [a], Yassine Riahi [a], Intisar Uddin [a], Ke Dai [a, *], Qiaoyun Huang [a]

[a] Key Laboratory of Arable Land Conservation (Middle and Lower Reaches of Yangtze River), Ministry of Agriculture and Rural Affairs, College of Resources and Environment, Huazhong Agricultural University, Wuhan, 430070, PR China
[b] Soil and Water Research Department, Nuclear Research Center, Atomic Energy Authority, Abou Zaabl, 13759, Egypt

HIGHLIGHTS

- Ternary complex of *S. oneidensis*-goethite-HA mightily enhanced Cr(VI) reduction.
- Precipitated $Cr(OH)_3$ and Cr_2O_3 were the final yields of reduction reaction.
- *S. oneidensis* can effectively reduce Fe(III)-oxides, oxidized HA and Cr(VI).
- Reduced HA acts as electron shuttles and accelerates the Cr(VI) reduction process.
- Reduced HA depressed goethite adhesion on bacterial cells.

GRAPHICAL ABSTRACT

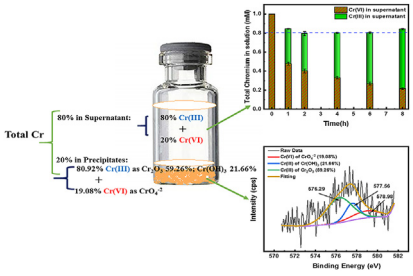

ARTICLE INFO

Article history:
Received 4 November 2019
Received in revised form
7 January 2020
Accepted 11 January 2020
Available online 11 January 2020

Handling Editor: Lena Q. Ma

Keywords:
Shewanella oneidensis MR-1
Goethite
Soil humic acid
Ternary complex
Bio-produced Fe(II)
Cr(VI) reduction

ABSTRACT

Microorganisms, iron minerals, and humic acid are widely common in the soil and water environment and closely interact within environmental processes. In this study, the Cr(VI) removal by *Shewanella* oneidensis MR-1 (*S. oneidensis*) was examined in the presence of goethite and humic acid (HA) to mimic the real environment situation. Scanning electron microscopy (SEM) combined with energy disperse spectroscopy (EDS), X-ray photoelectron spectroscopy (XPS), and electron paramagnetic resonance (EPR) technologies were used to probe the Cr(VI) reduction mechanism. Our results showed that *S. oneidensis* alone could reduce 65% of 1.0 mM Cr(VI) after 8 h of the reduction process. Meanwhile, Cr(VI) reduction rate was declined to 56% in the presence of goethite or humic acid. Contrary, the Cr(VI) reduction rate was mightily increased to 79% by the ternary complex of *S. oneidensis*-goethite-HA where reduced humic acid (HA_{red}) acted as electron shuttles and diminished the bacterial adhesion to the goethite surface thereby enhanced electron transfer and increased the extent of Cr(VI) reduction by 1.3 fold. XPS analysis indicated that Cr(VI) was reduced to Cr(III), and the final yields were $Cr(OH)_3$ and Cr_2O_3 precipitated on the surface of bacterial cells. *S. oneidensis* could also reduce Fe(III) in goethite to Fe(II), which in turn reduced Cr(VI). These results suggested that iron mineral-humic acid complex could enhance the microbial reduction of Cr(VI) and revealed the promotion role of HA in the Cr(VI) bioreduction process. This study affords inclusive insights on the Cr(VI) reduction kinetics and mechanisms in the most complicated systems.

* Corresponding author.
E-mail address: dk@mail.hzau.edu.cn (K. Dai).

https://doi.org/10.1016/j.chemosphere.2020.125902
0045-6535/

1. Introduction

Chromium is one of the most important contaminants of concern in the environment due to its extensive use in industrial activities such as metal processing, drilling, pigments, glass, ceramics, glues, textile dyeing, leather tanning, timber preservation, and ink manufacturing (Us Epa, 1984; Panagiotakis et al., 2015). In soil and water environment, chromium often exists in two stable oxidation forms, Cr(VI) and Cr(III). Hexavalent chromium form ($Cr_2O_7^{2-}$, $HCrO_4^-$ and CrO_4^{2-}) is highly mobile, toxic, and carcinogenic, whereas trivalent chromium usually has low solubility and strong affinity to soil components (Sarkar et al., 2013). Therefore, the reduction of Cr(VI) to Cr(III) is taken as an effective remediation strategy for Cr(VI)-contaminated sites (Brose and James, 2013).

Chromium remediation techniques such as chemical reducing agents (Gagrai et al., 2013), ion exchange (Cheng and Yan, 2010), adsorption (Johnston and Chrysochoou, 2016), electrochemical (Habibul et al., 2016), membrane filtration (Bao et al., 2015) and bioremediation (Khattar et al., 2015), have been adopted to detoxify and remove chromate from Cr(VI)-contaminated sites. However, among these techniques, bioremediation is taken as the most suitable, eco-friendly, and efficient technique (Cheng and Yan, 2010). Recent studies have demonstrated that various species of Cr(VI)-tolerant bacteria can reduce Cr(VI) whether via extracellular electron transfer (EES) or enzyme reductase ascribed to soluble proteins or cell membrane-bound proteins (Sathishkumar et al., 2017; Zheng et al., 2015). It has been reported that dissimilatory metal-reducing bacteria (DMRB) can use chromate as a terminal electron acceptor under anoxic conditions to reduce Cr(VI) (Wang et al., 2013). However, In soil and water environments, microorganisms are often adhered to iron minerals particles due to their opposite surface charges in most circumstances (Chenu and Stotzky, 2002). A previous study has demonstrated that more than 92% of *Pseudomonas putida* cells bound to the goethite mineral particles (Rong et al., 2010). Therefore, the effect of iron minerals on the microbial reduction of Cr(VI) should be considered.

Iron-bearing minerals which are ubiquitous in the soil and water environment have acquired a great attraction for ecological implementations and therapy of a wide range of contaminants and toxic substances. Cr(VI) can be reduced to Cr(III) by redox-active iron minerals existing in soil and subsurface sediment (Luan et al., 2015). However, the reduction rate is too slow in nature and depends on the Fe(II) content (Kwak et al., 2018). Previous studies have demonstrated that chemically reduced-clay minerals such as goethite, nontronite, hematite, and vermiculite can produce Fe(II) which declines Cr(VI) (Bishop et al., 2014; Parthasarathy et al., 2007). However, the chemical reducing agents such as dithionite is not available in the natural environment (Luan et al., 2015). DMRB can utilize iron minerals as terminal electron acceptors and generate Fe(II), which abiotically reduces Cr(VI) and immobilizes Cr(III) (Kumpiene et al., 2008). *Shewanella* oneidensis MR-1, a common DMRB widely existing in contaminated sites, has been reported to reduce Cr(VI) and iron minerals under anoxic conditions (Belchik et al., 2011; Wang et al., 2013). It has been confirmed that the direct electron transfer from DMRB to Fe(III) minerals is a vital pathway for microbial extracellular respiration (Shi et al., 2007). Proteins involved in such electron transfer, such as c-type cytochromes of *S. oneidensis*, are located in outer membranes of the DMRB. Thus, adhesion of the bacterial cells to Fe(III) minerals is essential for microbial mediated iron redox reactions. In these reactions, a Fe(II) was produced, which in turn reduce Cr(VI) via an indirect chemical reaction. Nevertheless, the coating of HA to iron minerals can alter the mineral surface properties, which affect their interaction with bacterial cells (Ouyang et al., 2018).

It has been reported that HA can catalyze certain reduction processes and adsorb to microorganisms and soil minerals (Tabatabai et al., 2005). Previous studies have demonstrated that HA can enhance microbial extracellular electron transfer which plays a critical role in Cr(VI) reduction (Li et al., 2009; Zhou et al., 2014). In the soil environment, Cr(VI) can be reduced by phenolic groups and carboxylic groups stored in HA (Zhang et al., 2019). DMRB is considered to use humic substances (HS) as electron shuttles by moving electrons to HS-quinone molecules, which could quickly reduce Fe(III) to Fe(II). Microorganisms can breathe under anaerobic conditions by moving electrons to strong phase quinone molecules in HS; therefore, reduced quinone moieties act as electron shuttles and accelerate the redox reactions (Roden et al., 2010; Stern et al., 2018).

Although microorganisms, iron minerals, and HA are commonly co-existed in Cr(VI)-contaminated environments, a little was known about their interface interaction and their potential influence on the Cr(VI) reduction process. Therefore, in this study, *Shewanella* oneidensis MR-1 was used to investigate Cr(VI) reduction kinetics and mechanisms in the presence of goethite and HA. In addition, the interaction between bacteria, goethite, and HA was examined and the fate of produced Cr was also explored.

2. Materials and methods

2.1. Materials

All chemicals used in the experiments were analytical reagent grade and water was supplied from a Milli-Q reference ultraviolet (UV)-water system. Cr(VI) stock solution (5.0 mM) was prepared by dissolving potassium chromate ($KCrO_4$; Sigma−Aldrich) in Milli-Q water. All butyl rubber stopper bottles, solutions, and growth media were sterilized prior to use. The reaction system was injected with nitrogen and carbon dioxide (N_2: CO_2 = 4:1) after each sampling to maintain the anoxic conditions. The initial pH 7 was maintained using NaOH/HCl adjustment. A 50 mM Bis-Tris propane (BTP, Sigma−Aldrich) solution was used as the buffer in all experiments. Stock solutions of sodium lactate (100 mM) were also prepared in Milli-Q water for use as an electron donor in all experiments. All stock solutions were stored at 4 °C prior to use.

2.2. Bacterial strain and culture conditions

Shewanella oneidensis MR-1, a model strain of DMRB which has been found in the Cr(VI)-contaminated environment was used for Cr(VI) reduction experiments (Venkateswaran et al., 1999). The test strain was purchased from China Culture Collection (CCTCC, AB 2013238). The bacterial cell was cultured in Luria-Bertani (LB) medium (5 g L^{-1} NaCl, 5 g L^{-1} yeast extract, 10 g L^{-1} tryptone) (Li et al., 2016). The strain was incubated in an orbital incubator at 28 °C with continuous trembling at 180 rpm until reaching to early exponential phase, the culture solution was inoculated to the same medium in an amount of 1% and cultured under the same conditions for 14 h to logarithmic long. The cells were collected by centrifugation at (8000 g, 4 °C, for 5 min), then washed three times with sterile 10 mM BTP buffer and re-suspended in the same solution as stock cultures. The resulting precipitate is formulated to have a dry weight of 10 g L^{-1} bacterial suspension. The optical density was measured at 600 nm absorbance (OD_{600}) by (Shimadzu UV-160A) UV visible spectrophotometer.

2.3. Goethite synthesis

The goethite mineral was synthesized according to Johnson (1990); Zhenghua et al. (2001). Briefly, 100 g of $Fe(NO_3)_3.9H_2O$ was dissolved in 1 L deionized water in a 2 L pre-sterilized

container. The dissolved solution was hydrated on a magnetic stirrer for 24 h (pH 1.6). Then a drop-wise solution of 2.5 M KOH was introduced until the solution pH reached 12. The resulting dense suspension was aged in the oven at 60 °C for five days. Then the goethite paste was dried at 60 °C on the oven. The synthesized mineral was ground to grains less than 154 μm in diameter, then placed in a vacuum desiccator, X-ray diffraction (XRD) was used for mineral characterization. Specific surface area (SSA) of goethite was analyzed using N_2 adsorption (Beijing Analytical Instrument Company, China). 10 g L^{-1} of minerals were suspended overnight in 10 mM BTP buffer (pH 7) and used as a stock suspension.

2.4. Soil HA extraction

The soil samples used for HA extraction were collected from the subtropical forest landscape located in central China (29° 23ʾ 32ʺ N, 114° 39ʾ 33ʺ E). The conditions of the land-form, climate and vegetation were described in detail by Jiang et al. (2017). The soil HA was extracted and purified using the standard method suggested by the International Humic Substances Society (IHSS) with minor modifications (Swift, 1996). Briefly, the soil samples were air-dried, ground, and then passed through a 2.0-mm sieve. 200 g of soil sample was suspended in 2.0 L of 0.1 M NaOH solution and shaken for 24 h at room temperature (~25 °C) under N_2. The supernatant liquid containing the soluble HA was separated by centrifugation at 16000*g* for 30 min. The residue was resuspended in 0.1 M NaOH, and the procedure was repeated five times. The combined solutions were filtered to remove solids, acidified with 6 M HC1 to pH 1, and allowed to stand at room temperature for 24 h. The precipitated HA fraction was separated from the supernatant by centrifugation. The HA was purified by the HC1/HF method until the ash content was less than 1.0%. The HA was dialyzed against distilled water until the dialysate was free of Cl and exhibited a neutral pH, then it was freeze-dried. 1.0 g L^{-1} of extracted soil humic acid was suspended overnight in 10 mM BTP buffer (pH 7) and used as a stock suspension.

2.5. Preparation of reaction system for Cr(VI) reduction process

Individual, binary, and ternary complexes of *S. oneidensis*, goethite, and HA were tested to reduce initial Cr(VI) concentrations ranging from 0.5 to 2.0 mM. All experiments were conducted in a 50-mL butyl rubber stopper bottles containing 25 mL reaction mixture of 1.0 g L^{-1} goethite, 1.0 g L^{-1} bacterial cell, 20 mg L^{-1} HA, and different Cr(VI) concentrations. Sodium lactate (25 mM) was added as an electron donor. The medium buffered with 10 mM BTP buffer and purged with N_2 gas for 10 min to ensure an anaerobic environment. The system pH was adjusted to the desired value (pH 7.0 ± 0.05) using NaOH/HCl. 2 mL aliquots were withdrawn at interval times and centrifuged at 8000 g, 4 °C for 5 min. Cr(VI) in the supernatant was estimated by a UV–vis spectrophotometer. Experimental results are taken from the average of a duplicate set up.

2.6. Analytical methods

2.6.1. Chromium (VI) estimation

Cr(VI) was measured using the diphenylcarbazide method at 540 nm by a UV/Vis spectrophotometer (Butler et al., 2015). A 2 mL of the reaction mixture was withdrawn and centrifuged at 8000 g for 5 min 1 mL of the supernatant was diluted with deionized water and then 0.5 mL of H_2SO_4 (50%, v/v) and H_3PO_4 (85%, w/w) was added. At last, 2 mL of diphenylcarbazide reagent (0.2%, w/v) was added and the resultant solution was shaken and allowed to stand 15 min for full color developing. UV–vis spectrophotometer (Shimadzu, Japan) was used to measure the absorbance at 540 nm. Total chromium in solution was measured by atomic absorption spectroscopy (Agilent 240AAFS). Cr(III) was computed from the difference between Cr(VI) and total chromium.

2.6.2. Mineral characterization

XRD analysis was used to verify the sample present phase. The XRD pattern of synthesized goethite mineral and the mineralogical changes on the mineral surface after reacting with bacteria, HA, and chromate was identified by the German Blake D8-ADVANCE, powder tableting method. X-ray diffractograms were acquired at 2θ angles from 10 to 80°, with a step size of 0.02° and 2 s counting time.

2.6.3. XPS analysis

X-ray photoelectron spectroscopy (XPS) studies were undertaken to determine the Cr oxidation states bound to cells. Data were analyzed by Avantage software. NIST website data was used to compare the peaks for Cr and Fe. XPS analysis of *S. oneidensis*-goethite-HA complex after reacting with Cr(VI) was performed by an XSAM800 X-ray photoelectron spectroscopy with Mg Kα. Carbon C1s (EBE = 284.8 eV) was used as the charge calibration standard.

2.6.4. Surface charge and surface site determination

Surface charge of *S. oneidensis*, goethite, HA and their complexes was determined using the Zeta plus 90 potentiometer from Brookhaven, USA. The zeta potential of the suspension of bacteria, minerals, humic acids, and their complexes was shown in Table 1. Each sample was assayed 3 times and averaged to the final zeta potential.

Potentiometric titration experiments were carried out to detect the surface sites on *S. oneidensis*, goethite, HA, and their complexes. 40 mL of the prepared complexes were added to the potentiometric titration pool. 10 mM NaCl was used as the electrolyte background. Table 1 shows the surface sites (the amount of OH^- consumed) for *S. oneidensis*, goethite, HA, and their complexes.

2.6.5. Functional groups assessment

Fourier-transform infrared spectroscopy (FTIR) was used to detect the functional groups on the surface of the bacterial cell. Precipitated samples of bacteria, bacteria-goethite, bacteria-HA, and bacteria-goethite-HA composites were lyophilized before and

Table 1
Zeta potential and surface sites (amount of OH^- consumed) for *S. oneidensis*, goethite, HA, and their complexes.

complex	Zeta Potential	Surface sites	
	Zeta (mv), 10 mM BTP, pH = 7	Concentration (g L^{-1})	Amount of OH^- consumed (mole/g), pH = 7
S. oneidensis	−6.48 ± 0.72	1.0	$3.41*10^{-3}$
Goethite	19.67 ± 0.32	1.0	$1.89*10^{-3}$
HA	−0.66 ± 0.24	0.02	$110.89*10^{-3}$
S. oneidensis-goethite	−8.52 ± 0.40	2.0	$1.98*10^{-3}$
S. oneidensis-HA	−9.30 ± 0.38	1.02	$3.336*10^{-3}$
S. oneidensis-goethite-HA	−9.80 ± 0.29	2.02	$1.705*10^{-3}$

after Cr(VI) reduction. KBr was mixed with the samples by a ratio (100: 1), fine-ground in an agate mortar. The samples were compressed (13 mm in diameter) and placed in a sample chamber of an infrared spectrometer (Nicolet AVAR 330) to obtain an infrared spectrum. The scanning wave number ranges from 800 to 1800 cm^{-1}, the scanning frequency is 128, 4 cm^{-1} resolution. The data were processed and analyzed using (Omnic 8.0) software.

2.6.6. SEM analysis

Scanning electron microscopy (SEM) and energy disperse spectroscopy (EDS) were used to observe the cell morphology and to assess the elemental mapping according to Dong et al. (2003). Centrifuged samples before and after Cr(VI) reduction by bacteria, bacteria-goethite, bacteria-HA, and bacteria-goethite-HA composites were subjected to fixation using 2.5% (v/v) glutaraldehyde for 12 h. The samples were centrifuged, washed three times and then dehydrated step by step with gradient concentrations of ethanol solution (30, 50, 70, 80, 95, and 100%) for 15 min at each stage. At last, cells were lyophilized and a suitable amount of dry powder sample adhered to the scanning electron microscope stage with a conductive adhesive. Cellular morphology was characterized by a Zeiss EV0 LS10 SEM (Carl Zeiss, Britain). The same samples were used to determine the elemental composition by EDS with an energy-dispersive X-ray analyzer.

2.6.7. Statistical analysis

All experiments in this research were carried out in duplicating setup. At least three separate bottles were set for one treatment. Each time three readings were taken, and their means and standard deviations were determined using (SPSS 7.5) software package. Error bars on graphs show the standard deviation.

3. Result and discussion

3.1. Characterization of goethite and HA

Synthesized goethite minerals were characterized by XRD and identified using the JCPDS PDF database for standard goethite (Fig. 1a). The characteristic diffraction peaks of goethite are 0.496, 0.418, 0.269, 0.244, 0.219, 0.172 nm, which are in good agreement with the standard goethite (Schwertmann and Cornell, 1992). The goethite particle size is around 500 nm (Fig. 3b), and the specific surface area measured by the BET method is 54.06 $m^2\ g^{-1,}$ and the point of zero charges (PZC) is about 8.7 which is inconsistent with previous studies (Jaiswal et al., 2013).

Previous studies demonstrated that the ability of HA to reduce Cr(VI) mainly depends on the kind of functional groups (Scaglia et al., 2013). FTIR spectras of extracted soil humic acid (HAs) were detected and compared with previous studies (Fig. 1b). The absorption strips at 3400 and 2920/2850 cm^{-1} are ascribed to O-H and aliphatic C-H vibration. Furthermore, the carboxyl group, integrated C=C or H-bonded C=O groups, and C-O stretching of phenolic groups was observed at 1720, 1614, and 1417 cm^{-1} absorption bands, respectively. Previous studies have also reported similar HAs fractions (Huang et al., 2012; Zhang et al., 2017). Detected functional groups revealed the role of humic acid in the Cr(VI) reduction process. Recent studies have suggested that the phenolic groups are the dominant functional groups that reduce Cr(VI) to Cr(III), which resulted in the formation of carbonyl/carboxyl groups (Hsu et al., 2009). Moreover, the carboxylic groups can maintain binding sites for Cr(III) (Ohta et al., 2012).

3.2. Surface charge and surface sites

Zeta potential of *S. oneidensis* and goethite (pH 7) were −6.48 and 19.67 mV, respectively (Table 1). After the combination, the zeta potential of *S. oneidensis*-goethite, *S. oneidensis*-HA, and *S. oneidensis*-goethite-HA complexes decreased to −8.52, −9.30, and −9.80 mV, respectively (Antelo et al., 2007). The coating of HA to goethite decreased its positive charge and promoted its aggregation leading to a weaker electrostatic attraction and lower surface area (Hong et al., 2015); therefore there was a limit potential for Cr(VI) adsorption on the surfaces of *S. oneidensis*-goethite-HA complex due to charge repulsions, and this hypothesis was confirmed by kinetic experiments. Additionally, the total chromium in solution in the ternary complex of *S. oneidensis*-goethite-HA is around 80% in different initial chromium concentration through reaction time (Fig. S1).

Table 1 also shows the surface sites of *S. oneidensis*, goethite, HA, and their complexes. The OH^- consumed during the automatic potentiometric titration represents the surface site concentration of the titrated substance (Fig. S2). The lower surface sites, the better buffer performance of the system, and richer functional groups (Ueshima et al., 2008). After the combination of *S. oneidensis*, goethite, and HA, the surface sites clearly depressed and became less than the *S. oneidensis* surface site, indicating that there is a

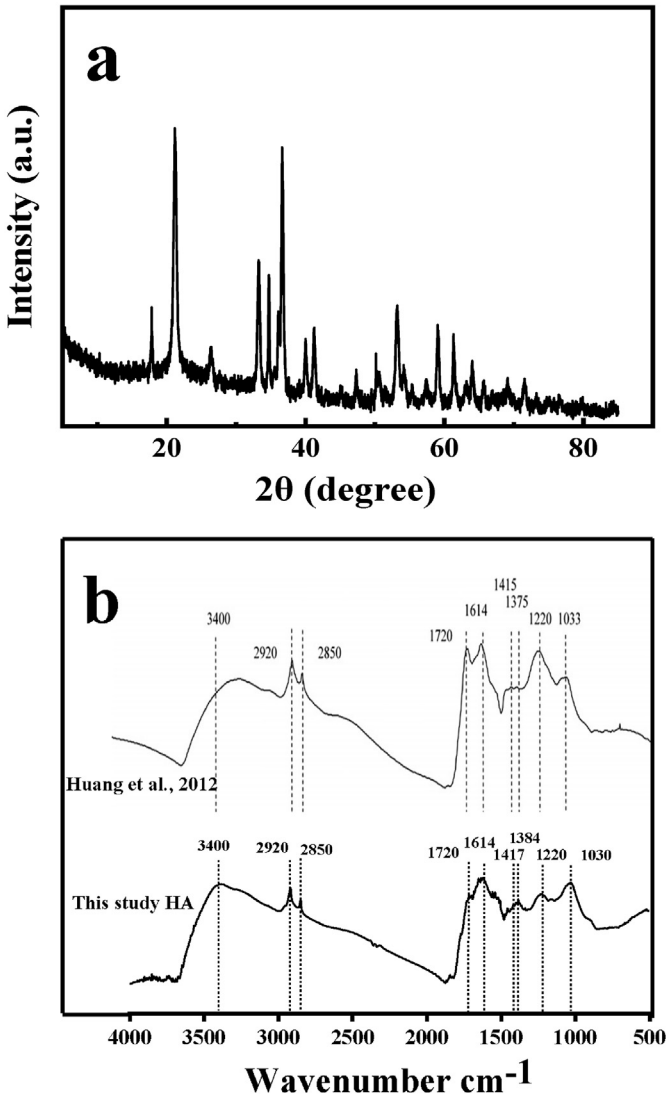

Fig. 1. XRD patterns of synthesized goethite mineral (a); and FT-IR spectra of extracted soil humic acid (HAs), compared with a previous characterized HA.

prosperity of the sites in the compounding reaction, which probably affects the Cr(VI) reduction process (Zhang et al., 2011).

3.3. Cr(VI) reduction kinetics

The effect of initial Cr(VI) concentration ranged from 0.5 to 2 mM on the Cr(VI) reduction by *S. oneidensis*, goethite, HA, and their complexes was determined (Fig. 2). As the initial chromate concentration increased, the Cr(VI) reduction by *S. oneidensis* decreased (Fig. 2a) (Liu et al., 2016). Within 1 h, 0.5 mM of initial Cr(VI) concentration was completely reduced whereas, after 8 h, *S. oneidensis* could reduce 65, 42, and 29% of 1.0, 1.5, and 2.0 mM of initial Cr(VI) concentration respectively. These results suggest that Cr(VI) reduction at high concentrations was limited due to chromate toxicity, proving that *S. oneidensis* is highly prone to chromate toxicity, which causes growth inhibition (Liu et al., 2019; Viamajala et al., 2004). The result of the pseudo-first-order kinetic model fitting also revealed that the Cr(VI) reduction rate declined by increasing the initial chromate concentration (Fig. S3; Table S1 $R^2 > 0.8$).

Cr(VI) removal by goethite minerals did not exceed 10% (Fig. 2b), which probably attributed to the chromate adsorption on goethite

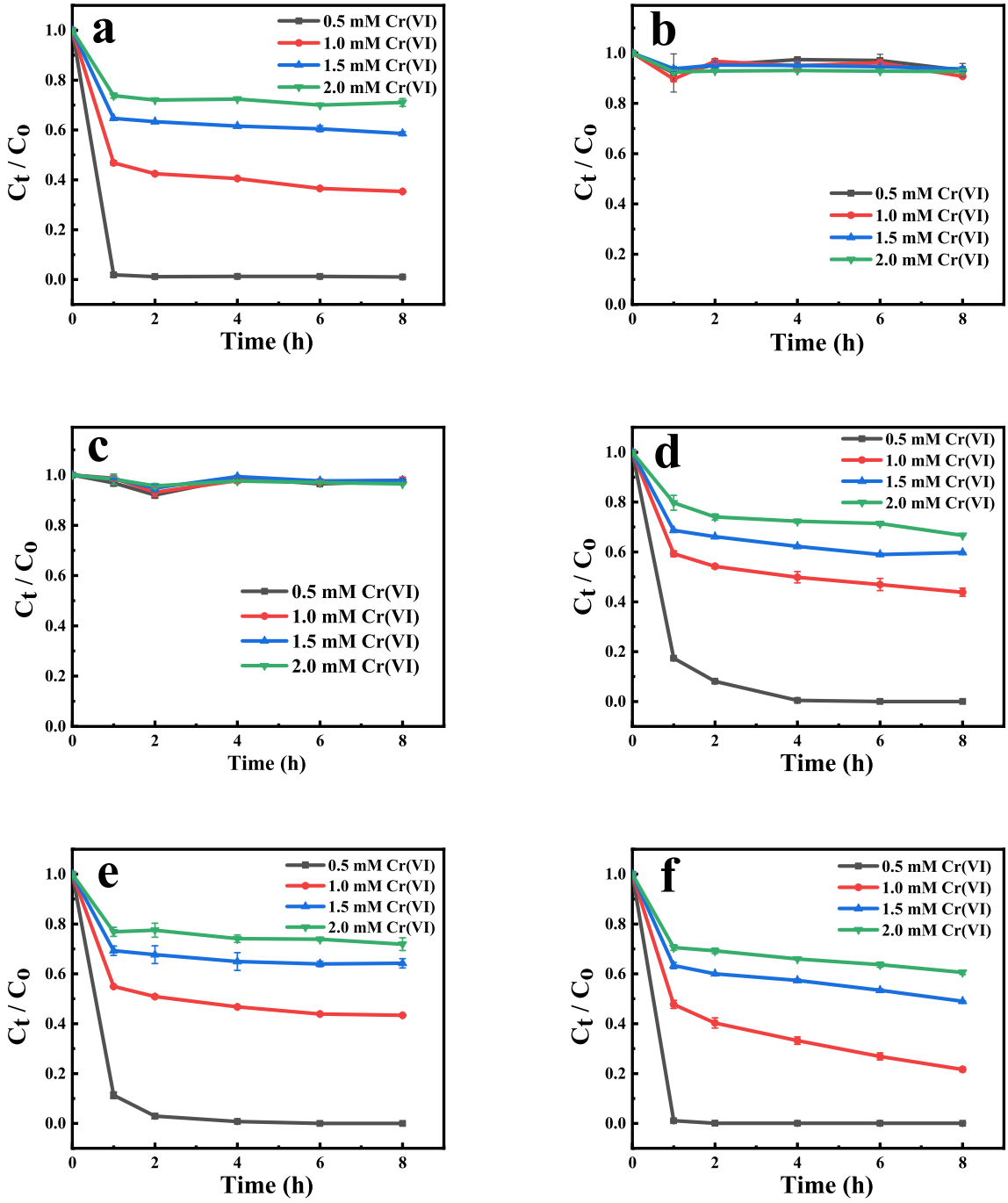

Fig. 2. Effect of initial Cr(VI) concentration (0.5, 1.0, 1.5, and 2.0 mM) on its reduction by S. oneidensis (a); goethite (b); humic acid (c); S. oneidensis-goethite (d); S. oneidensis-HA (e); and S. oneidensis-goethite-HA complexes (f) in 25 ml mixture (pH 7) containing 1 g L^{-1} bacterial concentration, 1 g L^{-1} goethite minerals, 20 mg L^{-1} HA, 10 mM BTP buffer, 25 mM sodium lactate. Error bars indicate ± standard error of the mean of duplicate assays and are smaller than symbols were not visible.

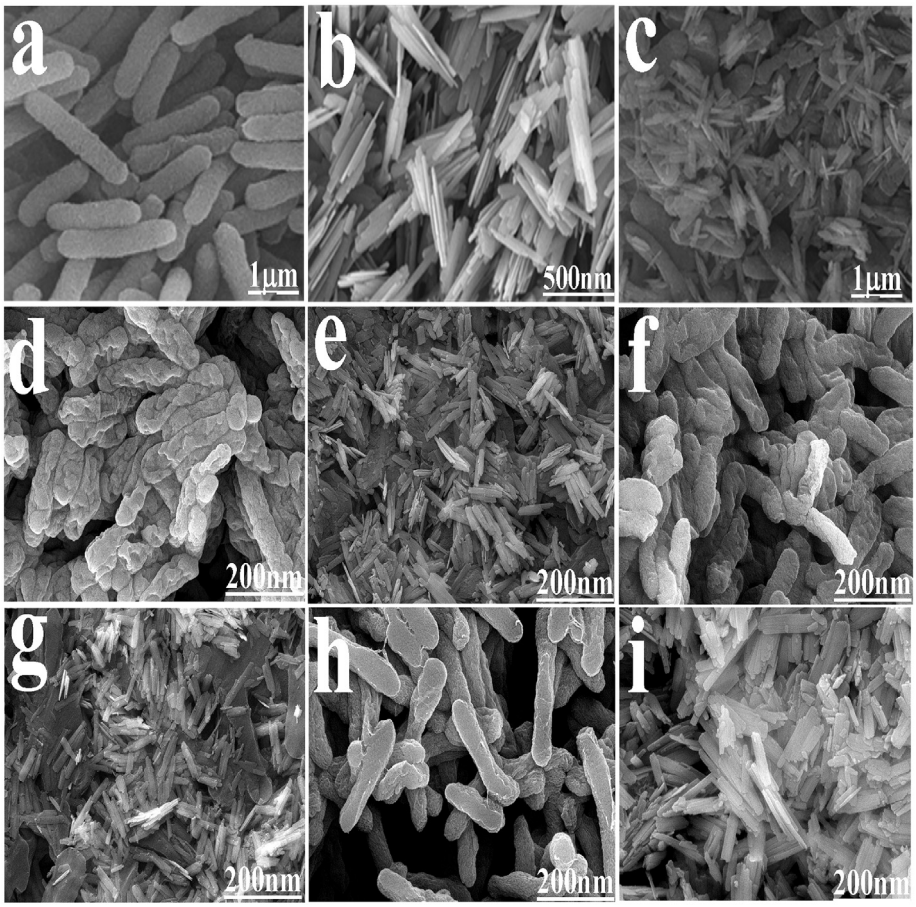

Fig. 3. SEM images of *S. oneidensis* (a); goethite (b); *S. oneidensis*-goethite (c); *S. oneidensis*-HA (d); *S. oneidensis*-goethite-HA (e); *S. oneidensis*-Cr(VI) (f); *S. oneidensis*-goethite-Cr(VI) (g) *S. oneidensis*-HA-Cr(VI) (h); and *S. oneidensis*-goethite-HA-Cr(VI) (i).

minerals or the abiotic reduction by released Fe(II) (Jiang et al., 2014; Meng et al., 2018). Oxidized humic acid (HA_{ox}) alone could not reduce Cr(VI) as well (Fig. 2c) probably as the Cr(VI) reduction process by HA mainly depends on the system pH and exhibits slow reduction rate at neutral pH values (Gu and Chen, 2003; Nakayasu et al., 1999). Goethite minerals slightly inhibited Cr(VI) bioreduction in the binary complexes of *S. oneidensis*-goethite, probably due to the obstruction of electron transfer as goethite covered and blocked the surface cell as shown and confirmed by SEM images (Fig. 3c) (Zhao et al., 2019, 2018). The binary complex of *S. oneidensis*-HA probably interrupted electron transfer since HA acted as a competitive electron acceptor; therefore HA led to a slight inhibition of Cr(VI) bioreduction (Fig. 2e) (Stone et al., 2007).

In contrast, the ternary complex of *S. oneidensis*-goethite-HA strongly stimulated Cr(VI) bioreduction (Fig. 2f). In this case, HA_{red} played a crucial role since the coating of HA depressed the positive charge of goethite, thereby led to a weaker electrostatic attraction and lower available surface area, which probably contributed to the lower attachment to bacterial cell that reduced the blocking of electron transfer; therefore, the ternary complex promotes Cr(VI) reduction process (Hong et al., 2015). HA inhibited the attachment of *S. oneidensis* to the goethite surface due to the competition between HA and bacteria for the same adhesion sites on the goethite surface (Foppen et al., 2008). Additionally, HA_{red} acted as electron shuttles and accelerated the electron transfer to Cr(VI). Consequently, the ternary complex of *S. oneidensis*-goethite-HA enhanced the Cr(VI) reduction process (Meng et al., 2018).

3.4. Scanning electron microscopy (SEM)

Scanning electron microscopy (SEM) analysis was performed to determine the morphology of *S. oneidensis* and its complexes with goethite and HA before and after reacting with 1.0 mM Cr(VI) for 8 h. SEM images showed that, before reacting with chromate, the cells were regular rod-shaped with smooth surfaces (Fig. 3a). Meanwhile, after reacting with chromate ions, the bacterial cells became atrophic with a shrunken-surface shape and cracks formation was also observed (Fig. 3f). This observation revealed that chromate stress changed cell morphology and had a toxic effect on *S. oneidensis* (Kang et al., 2014). In the presence of chromate, bacterial cells were co-compacted to show more elasticity and flexibility (Fig. 3f), while the cells seemed to be clear and separated without Cr(VI) (Bhattacharya and Gupta, 2013). These results interpreted the cell morphology changes due to chromate stress (Chatterjee et al., 2011).

SEM images of *S. oneidensis*-goethite complex showed that goethite minerals covered the surface of *S. oneidensis* (Fig. 3c and g), which probably disrupted electron transfer and thereby inhibited Cr(VI) bioreduction (Zhao et al., 2019, 2018). Likewise, SEM images of *S. oneidensis*-HA complex showed that the bacterial cells lost their regular shapes, some appeared to be broken, and irregular cell fragments were observed (Fig. 3d and h), revealing that HA inhibited the cell activity and therefore, decreased Cr(VI) reduction rate (Zhao et al., 2018). SEM images of *S. oneidensis*-goethite-HA showed that the cell surface was partially covered with goethite (Fig. 3e and i), as HA diminished the bacterial adhesion to the

goethite surface due to the competition between HA and bacteria for the same adsorption sites on the goethite surface (Foppen et al., 2008), which allowed the electron transfer to chromate and thus, stimulated Cr(VI) reduction rate.

3.5. Surface functional groups

The FTIR spectras of *S. oneidensis* combined with goethite and humic acid before and after reacting with Cr(VI) were determined (Fig. 4). The main absorption peaks were C=O stretching vibration (amide I band) at 1655 cm^{-1}, N-H bending vibration and C-N stretching vibration (amide II band) at 1540 cm^{-1}, symmetrical deformation of H-C-H, C-O-H at 1456 cm^{-1}, bending vibration of H-C-C group at 1387 cm^{-1}, P=O asymmetric stretching vibration at 1238 cm^{-1}, symmetric stretching vibration of C-O-C in glycosidic bonds at 1079 cm^{-1} (Elzinga et al., 2012; Tribe et al., 2006). After the combination of *S. oneidensis* and goethite, the binary and ternary complexes exhibited a characteristic absorption peak of goethite at 888 cm^{-1} assigned to C-H bending. The characteristic absorption peaks on the composite did not shift significantly or result in the emergence of new feature peaks. The main characteristic absorption peaks of *S. oneidensis* are C=O (amide I), and N-H/C-N (amide II). The trend of weakening peak intensity speculated that Cr(VI) mainly reacted with *S. oneidensis* on the complexes, confirming the crucial role of certain functional groups on the surface of *S. oneidensis* such as carboxyl and amide groups in the metal-binding process (Kang et al., 2015).

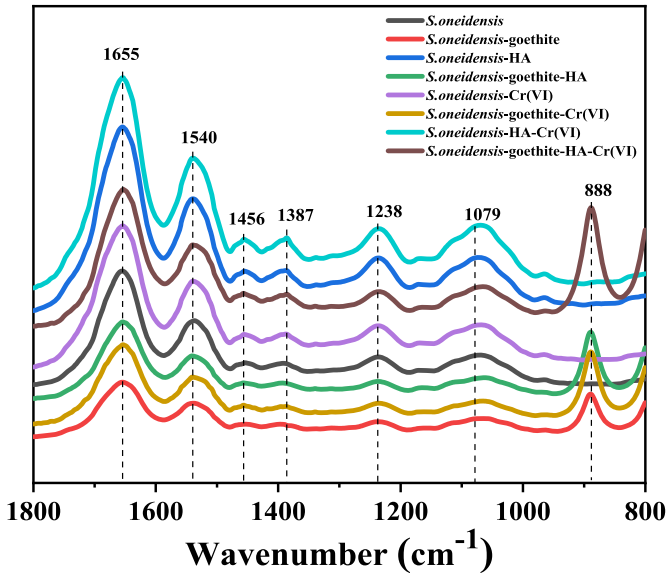

Fig. 4. FT-IR spectra of Shewanella oneidensis MR-1, and its binary and ternary complexes with goethite, and HA before and after reacting with 1 mM Cr(VI) for 8 h.

3.6. The fate of chromium and iron cycling

The full XPS survey scan for the ternary complex of *S. oneidensis*-goethite-HA before and after reacting with 1.0 mM Cr(VI) for 8 h was determined (Fig. 5). The atomic percentage of C 1s, O 1s, Cr 2p, and Fe 2p were 52.32, 39.69, 0.51, and 7.48%, respectively (Fig. 5b). The atomic percentage of Fe 2p before and after the Cr(VI) reduction process was slightly reduced from 8.71 to 7.48%, confirming the crucial role of iron in the chromium reduction process (Fig. 5a and b). The C 1s spectra indicated that the plurality of C in *S. oneidensis*-goethite-HA composite was represented as C-H or C-C and O-C=O with a tiny amount of C-O-C (Fig. 6a). Cr 2p XPS analysis obviously illustrated that the final yields of the Cr(VI) reduction process were $Cr(OH)_3$ and Cr_2O_3 precipitates (Fig. 6c) represent about 80% of solid precipitates, which is consistent with the reduction kinetic results (Fig. 2f) revealing that there is a few Cr(VI) adsorbed on the solid surface (Liu et al., 2019; Tian et al., 2016). The Fe 2p spectrum of the *S. oneidensis*-goethite-HA complex (Fig. 6d) revealed the existence of both Fe(II) (725.41 eV) attributed to $FeCr_2O_4$ (27.06%) and Fe(III) (710.79, 711.7, and 713.56 eV) represented by Fe_2O_3 (9.75%), octahedral Fe(III) (36.15%) and tetrahedral Fe(III) (20.71%) respectively (Liu et al., 2019; Lu et al., 2018).

The relative distribution of Fe speciation and alternation series in the goethite mineral and its complexes with *S. oneidensis* and HA were figured out (Fig. 7). Goethite mineral has 29.97% of octa Fe(II) (Fig. 7a). After the combination of *S. oneidensis* with goethite, the octa Fe(II) increased to 34.65% revealing the electron transfer from bacteria to goethite to reduce Fe(III) to Fe(II) (Fig. 7b). In the ternary complex of *S. oneidensis*-goethite-HA, Octa Fe(II) reached 31.77% (Fig. 7c), suggesting that HA_{ox} competed with goethite mineral to accept electrons transferred from bacteria (Stone et al., 2007). Once the ternary complex reacted with Cr(VI), Fe(II) of $FeCr_2O_4$ was strongly decreased to 27.06%, confirming that two redox cycles of chromium and iron were occurred at the same time through the abiotic Cr(VI) reduction process according to the following formula:

$$3Fe(II) + Cr(VI) \rightarrow 3Fe(III) + Cr(III) \quad (1)$$

$$Cr(III) + OH^- \rightarrow Cr(OH)_3 \quad (2)$$

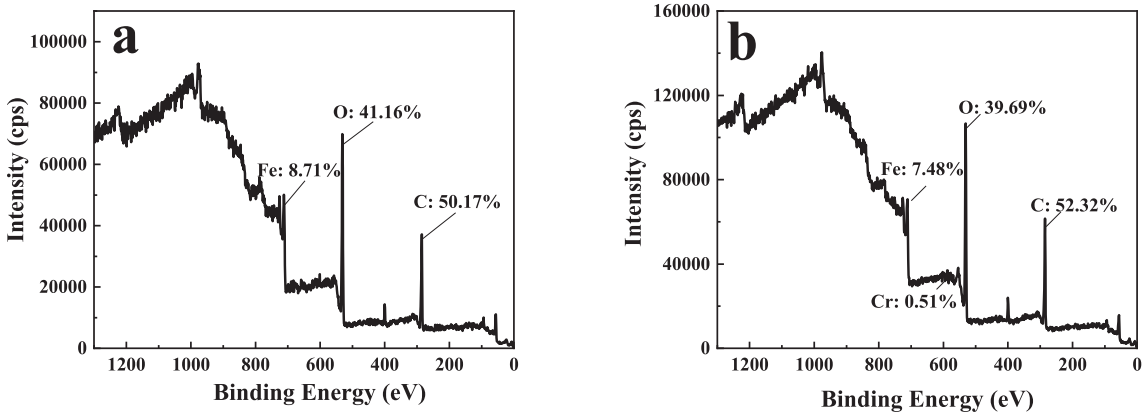

Fig. 5. Full XPS survey scan of the ternary complex of S. oneidensis-goethite-HA before (a); and after reacting with Cr(VI) (b).

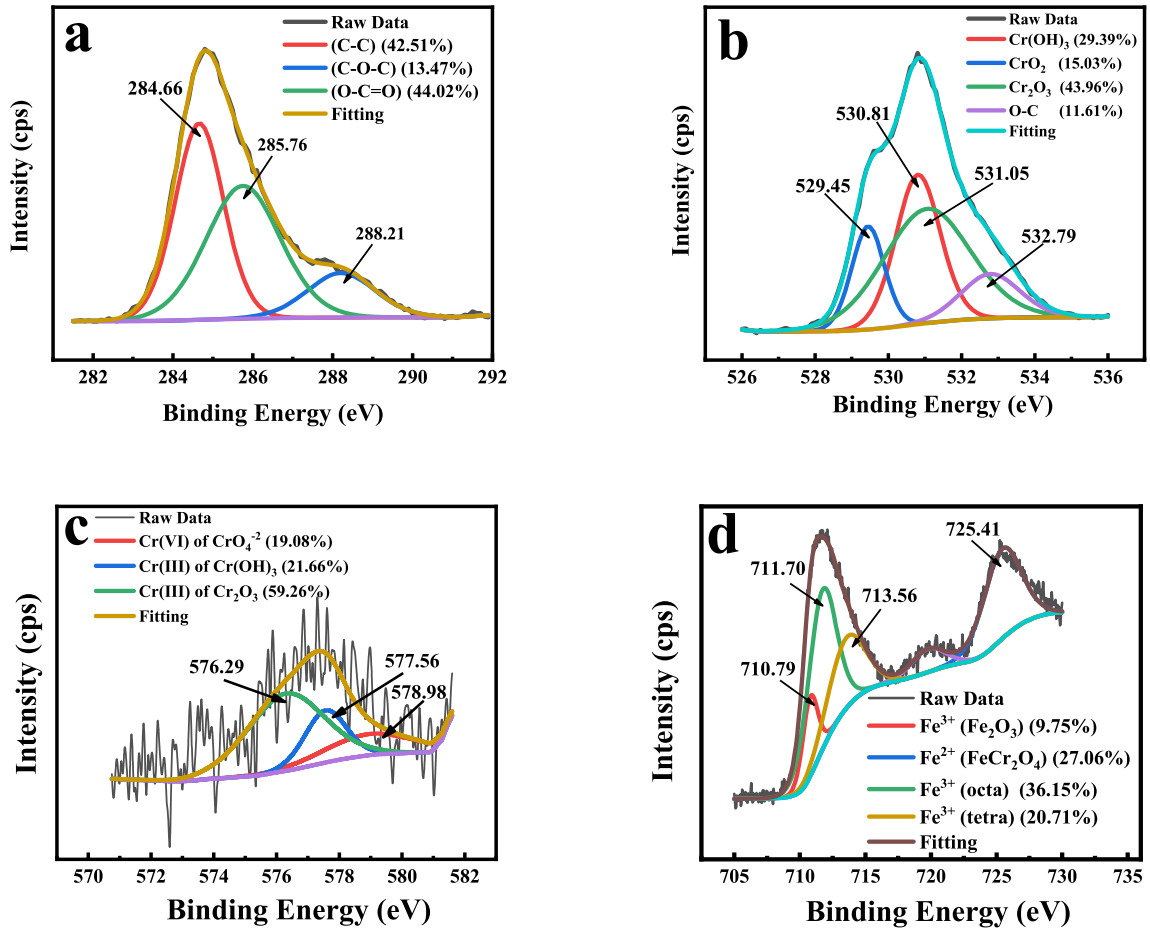

Fig. 6. XPS spectra of C 1s (a); O 1s (b); Cr 2p (c); and Fe 2p (d) from the fractured surfaces of S. oneidensis-goethite-HA after reacting with 1 mM Cr(VI) for 8 h. All spectra were referenced to a C 1s photopeak at 284.8 eV.

These results emphasized that Fe(II) generated from goethite mineral had a vital role and rapidly reduced Cr(VI) (Fig. 7b) (Kwak et al., 2018). Furthermore, the total iron content was decreased during Cr(VI) reduction process (Fig. S4). Moreover, XPS analysis deeply confirmed that the composition of the newly-formed surface layer consists of Fe(III)-Cr(III) (oxy)hydroxides with Cr(VI) adsorbed on the outside surface (Huang et al., 2018).

3.7. Analyses of precipitated solid leachate

Energy disperses spectroscopy (EDS) analysis was performed in the leachate to prove the Cr(VI) reduction process. EDS images illustrated that the precipitated solid complexes contain signal peaks of carbon, oxygen, phosphorus, sulfur, potassium, and silicon, which were mainly resulting from the components of the cell membrane, e.g., polysaccharides and proteins (Guria et al., 2014). EDS elemental analysis of the complexes of *S. oneidensis*-goethite-HA, *S. oneidensis*-HA-Cr(VI), and *S. oneidensis*-goethite-HA-Cr(VI) was estimated (Table S.2). Clear sharp chromium peaks were observed in the spectrum of *S. oneidensis*-HA-Cr(VI) (Fig. 8b). Meanwhile, no chromium peaks were detected in the EDS spectra of the ternary complex of *S. oneidensis*-goethite-HA (Fig. 8c), proving the efficient reduction of Cr(VI) through the ternary complex (Kumari et al., 2015). Previous studies speculated that the chromium compound probably exists as crystalline or amorphous structures, which can not be assessed in EDS spectra otherwise, the secondary metabolites produced during bacterial culture cells could compete with bacteria for Cr(III) attachment and as a result, soluble chromium complexes could be produced; therefore, the chromium immobilization ratio is declined (Cheng and Yan, 2010; Kumari et al., 2015).

XRD spectrum of goethite after combining with *S. oneidensis*, HA, and reacting with Cr(VI) for 8 h did not exhibit significant changes (Fig. S5). The peak position and relative intensity demonstrated that no significant changes occurred in the binary and ternary complexes. These results suggested that goethite mineral is more stable in short-term reactions and maybe exhibits alternation peaks in long-term reaction composites (Zhou et al., 2018).

3.8. Electron paramagnetic resonance (EPR)

EPR analysis was employed to examine the reactive reductive intermediate Cr valence states during the Cr(VI) reduction process. Fig. 9 shows the EPR spectrum of the *S. oneidensis*-goethite-HA complex after reacting with Cr(VI) for 3 h. A significant signal appears at g = 1.98 attributed to Cr(V); this finding revealed that there

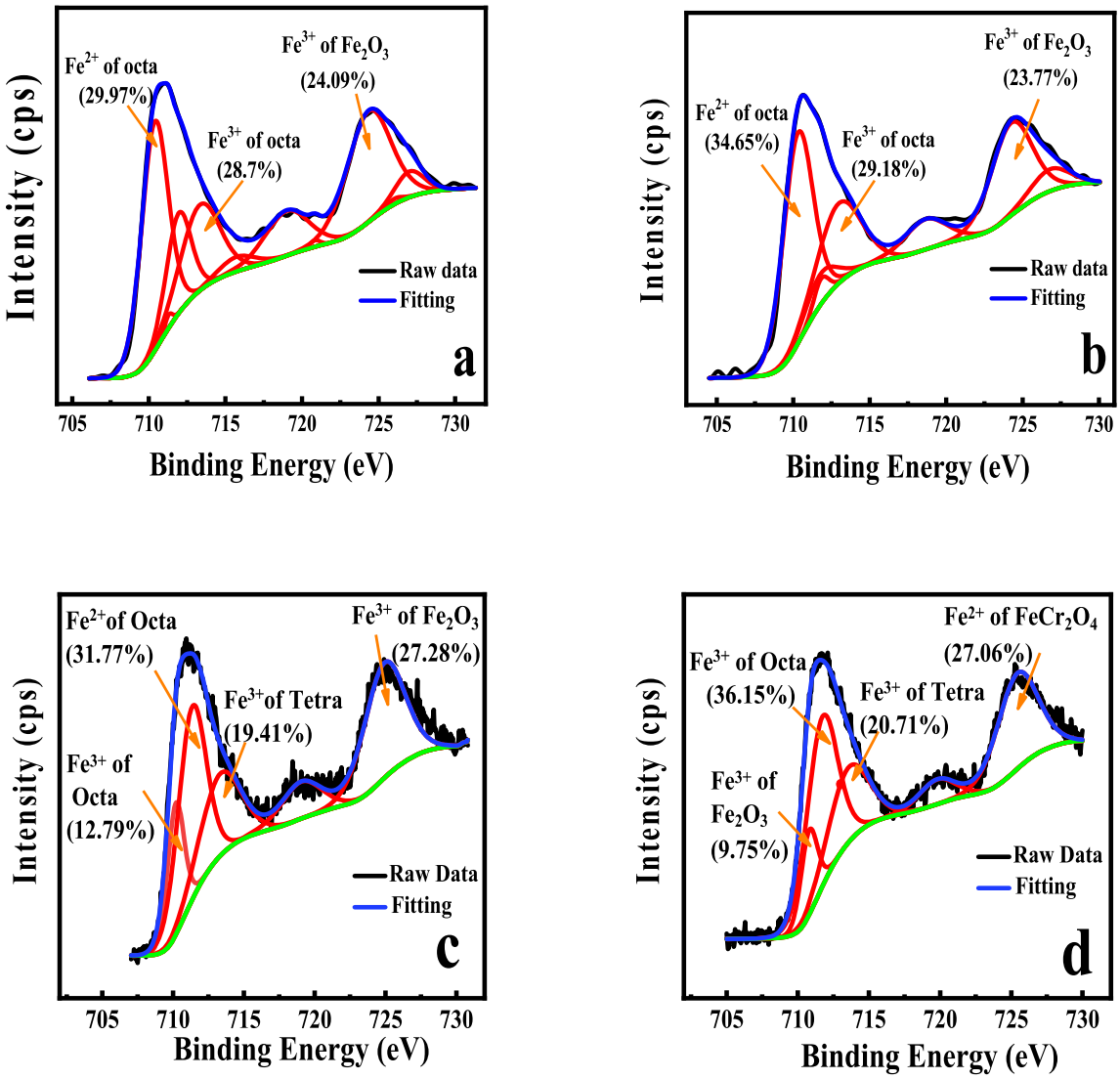

Fig. 7. Fe 2p XPS spectra of goethite (a); *S. oneidensis*-goethite (b); *S. oneidensis*-goethite-HA (c); and *S. oneidensis*-goethite-HA-Cr(VI) (d). All spectra were referenced to a C 1s photopeak at 284.8 eV.

was an intermediate valence state of Cr(V) during the reduction of Cr(VI) by *S. oneidensis*-goethite-HA. Therefore, EPR analysis provided supporting evidence and demonstrated that Cr(VI) reduction is a two-step electron transfer process (Liu et al., 2016; Weckhuysen and Schoonheydt, 1994). This pathway was in agreement with several previous studies that confirmed in various Cr(VI)-reducing bacterial strains (Myers et al., 2000; Wani et al., 2007).

3.9. Cr(VI) reduction mechanism in the ternary complex of *S. oneidensis*-goethite-HA

Chromium reduction pathways through the ternary complex of *S. oneidensis*-goethite-HA were shown in Fig. 10. Each component has its role to decrease Cr(VI) in the ternary complex reaction. First *S. oneidensis* could reduce Cr(VI) to Cr(III) by direct extracellular electron transfer (EET). Additionally, it was also able to reduce Fe(III) and HA_{ox} to Fe(II) and HA_{red}, respectively. Second, goethite is a Fe(III) source that can be reduced to produce Fe(II) which took part in the Cr(VI) reduction process. Third, HA_{red} not only acted as electron shuttles among *S. oneidensis*, goethite, and Cr(VI), which accelerate the reduction of Fe(III) and Cr(VI) but also hindered the bacterial cells from goethite adhesion which prevent the electron transfer blocking (Zhao et al., 2019, 2018). Thus, the ternary complex of *S. oneidensis*-goethite-HA could enhance Cr(VI) reduction through parallel biotic and abiotic processes, where HA_{red} was taken as the watchword in the ternary complex of the reaction system.

4. Conclusions

In this study, Cr (VI) reduction by *Shewanella oneidensis* MR-1 in the presence of goethite and HA was investigated. The results showed that *S. oneidensis* can reduce Cr(VI) to Cr(III) and Fe(III) in goethite mineral to Fe(II), which in turn quickly reduces Cr(VI). The

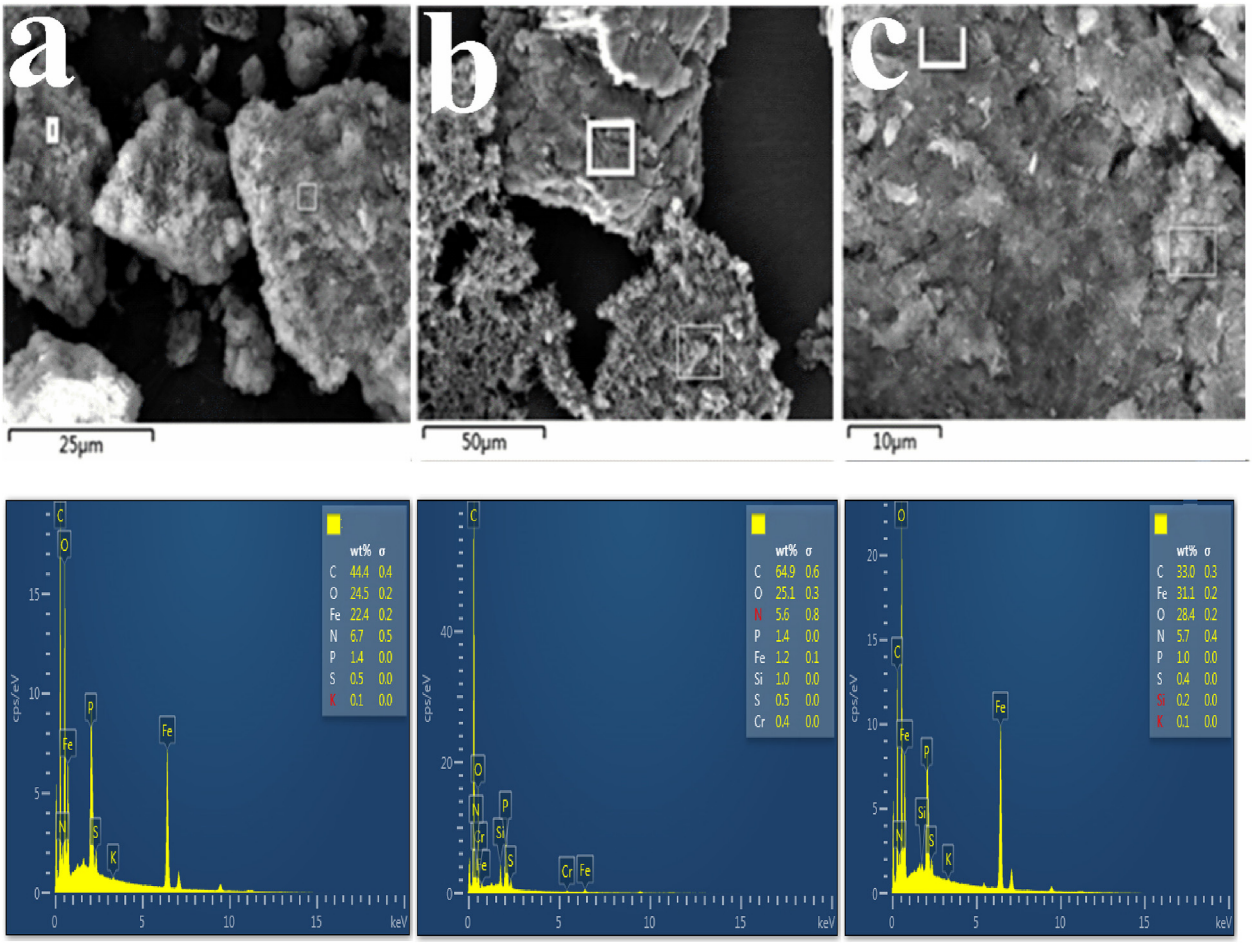

Fig. 8. EDS images and elements mapping of *S. oneidensis*-goethite-HA (a); *S. oneidensis*-HA-Cr(VI) (b); and *S. oneidensis*-goethite-HA-Cr(VI) (c).

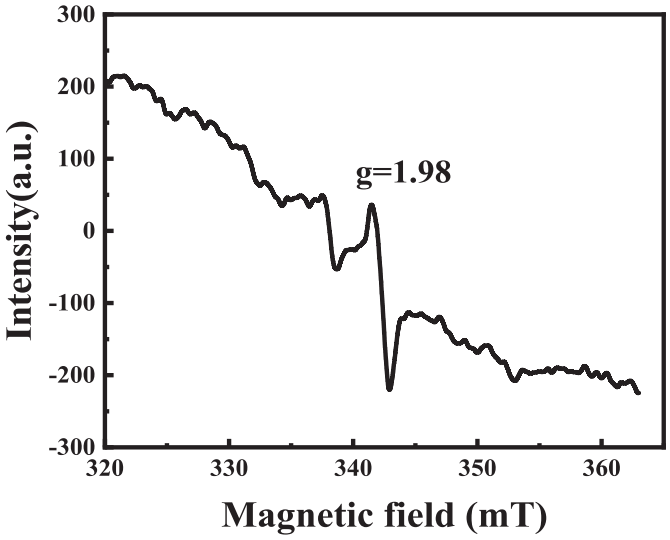

Fig. 9. EPR spectrum of S. oneidensis-goethite-HA during the reduction of Cr(VI).

Cr(VI) reduction rates decreased with the increase of the initial Cr(VI) concentrations due to the chromate toxicity on bacterial cells. Binary complexes of *S. oneidensis*-goethite and *S. oneidensis*-HA slightly inhibited Cr(VI) reduction since goethite covered the cell surface and interrupted the electron transfer, whereas HA competed with Cr(VI) to accept electron transferred from bacterial cells. The ternary complex of *S. oneidensis*-goethite-HA strongly enhanced Cr(VI) reduction rate. XPS analysis confirmed that the final yields of reduction reaction were $Cr(OH)_3$ and Cr_2O_3 precipitated on the cell surface. Our results suggested that HA could overcome the goethite inhibition which blocks the active sites on bacterial surfaces that transfer electrons to the extracellular environment. Therefore, Fe(III) minerals and humic acid drastically promoted Cr(VI) bioreduction. This research offers a novel approach to remove Cr(VI) from Cr(VI)-contaminated sites.

4.1. Environmental implications

Our study provides promising insights to monitor the fate of Cr(VI) as well as its reduction mechanisms in more complicated environmental systems, including microorganisms, iron minerals, and humic acid. Such knowledge affords possible implications for Cr(VI) reduction kinetics in Cr(VI)-contaminated systems. The results presented herein suggest that *S. oneidensis*-goethite-HA combination could be an efficient way to reduce high toxic Cr(VI) to

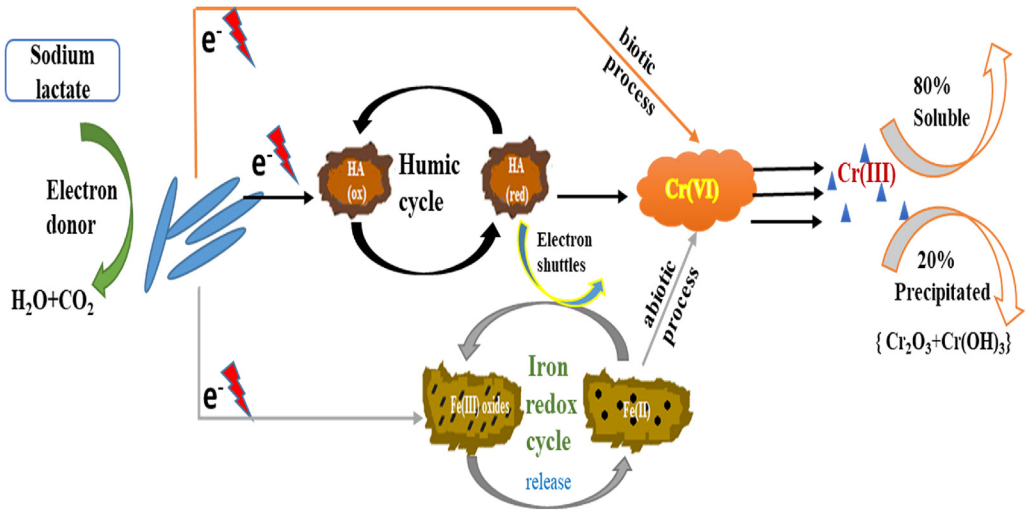

Fig. 10. Chromium reduction pathways through the ternary complex of *S. oneidensis*-goethite-HA.

lower Cr(III). Thus, it may provide a potential novel approach for Cr(VI) remediation strategies in high chromate contaminated sites through friendly environmental processes.

Supplementary data

The supplementary data is available: surface sites (potentiometric titration curves), EDS elemental mapping of binary and ternary complexes, pseudo-first-order kinetic model fitting and reduction efficiency and fitting parameters of reaction kinetics, Total Fe concentration in solution during Cr(VI) reduction process and XRD spectrum of goethite after combining with *S. oneidensis*, HA and reacting with Cr(VI).

Declaration of interests

The authors declare that they have no known competing for financial interests or personal relationships that could have appeared to influence the work reported in this paper.

CRediT authorship contribution statement

Abdelkader Mohamed: Project administration, Investigation, Methodology, Writing - original draft, Writing - review & editing. **Lu Yu:** Investigation, Methodology. **Yu Fang:** Data curation, Formal analysis. **Noha Ashry:** Investigation, Methodology, Software. **Yassine Riahi:** Data curation, Resources, Software. **Intisar Uddin:** Investigation, Methodology, Formal analysis. **Ke Dai:** Conceptualization, Funding acquisition, Supervision, Validation, Visualization, Writing - review & editing. **Qiaoyun Huang:** Supervision, Validation, Visualization, Writing - review & editing.

Acknowledgments

The research was financially supported by the National Natural Science Foundation of China (41671230).

Appendix A. Supplementary data

Supplementary data to this article can be found online at https://doi.org/10.1016/j.chemosphere.2020.125902.

References

Antelo, J., Arce, F., Avena, M., Fiol, S., López, R., Macías, F., 2007. Adsorption of a soil humic acid at the surface of goethite and its competitive interaction with phosphate. Geoderma 138, 12–19. https://doi.org/10.1016/j.geoderma.2006.10.011.

Bao, Y., Yan, X., Du, W., Xie, X., Pan, Z., Zhou, J., Li, L., 2015. Application of amine-functionalized MCM-41 modified ultrafiltration membrane to remove chromium (VI) and copper (II). Chem. Eng. J. https://doi.org/10.1016/j.cej.2015.06.094.

Belchik, S.M., Kennedy, D.W., Dohnalkova, A.C., Wang, Y., Sevinc, P.C., Wu, H., Lin, Y., Lu, H.P., Fredrickson, J.K., Shi, L., 2011. Extracellular reduction of hexavalent chromium by cytochromes MtrC and OmcA of Shewanella oneidensis MR-1. Appl. Environ. Microbiol. 77, 4035–4041. https://doi.org/10.1128/AEM.02463-10.

Bhattacharya, A., Gupta, A., 2013. Evaluation of Acinetobacter sp. B9 for Cr (VI) resistance and detoxification with potential application in bioremediation of heavy-metals-rich industrial wastewater. Environ. Sci. Pollut. Res. 20, 6628–6637. https://doi.org/10.1007/s11356-013-1728-4.

Bishop, M.E., Glasser, P., Dong, H., Arey, B., Kovarik, L., 2014. Reduction and immobilization of hexavalent chromium by microbially reduced Fe-bearing clay minerals. Geochem. Cosmochim. Acta 133, 186–203. https://doi.org/10.1016/j.gca.2014.02.040.

Brose, D.A., James, B.R., 2013. Hexavalent chromium reduction by tartaric acid and isopropyl alcohol in mid-atlantic soils and the role of Mn(III,IV)(hydr)oxides. Environ. Sci. Technol. 47, 12985–12991. https://doi.org/10.1021/es401903s.

Butler, E.C., Chen, L., Hansel, C.M., Krumholz, L.R., Elwood Madden, A.S., Lan, Y., 2015. Biological versus mineralogical chromium reduction: potential for reoxidation by manganese oxide. Environ. Sci. Process. Impacts 17, 1930–1940. https://doi.org/10.1039/c5em00286a.

Chatterjee, S., Ghosh, I., Mukherjea, K.K., 2011. Uptake and removal of toxic Cr(VI) by Pseudomonas aeruginosa: physico-chemical and biological evaluation. Curr. Sci. 101, 645–652.

Cheng, Y., Yan, F., 2010. Bioremediation of Cr (VI) and immobilization as Cr (III) by. Ochrobactrum anthropi 44, 6357–6363.

Chenu, C., Stotzky, G., 2002. Interactions between microorganisms and soil particles: an overview. In: Huang, P.M., Bollag, J.M., Senesi, N. (Eds.), Interactions between Soil Particles and Microorganisms: Impact on the Terrestrial Ecosystem. Wiley, New York, NY, pp. 3–40.

Dong, H., Kostka, J.E., Kim, J., 2003. Microscopic evidence for microbial dissolution of smectite. Clay Clay Miner. https://doi.org/10.1346/CCMN.2003.0510504.

Elzinga, E.J., Huang, J.H., Chorover, J., Kretzschmar, R., 2012. ATR-FTIR spectroscopy study of the influence of ph and contact time on the adhesion of shewanella putrefaciens bacterial cells to the surface of hematite. Environ. Sci. Technol. 46, 12848–12855. https://doi.org/10.1021/es303318y.

Foppen, J.W., Liem, Y., Schijven, J., 2008. Effect of humic acid on the attachment of Escherichia coli in columns of goethite-coated sand. Water Res. 42, 211–219. https://doi.org/10.1016/j.watres.2007.06.064.

Gagrai, M.K., Das, C., Golder, A.K., 2013. Reduction of Cr(VI) into Cr(III) by Spirulina dead biomass in aqueous solution: kinetic studies. Chemosphere. https://doi.org/10.1016/j.chemosphere.2013.08.021.

Gu, B., Chen, J., 2003. Enhanced microbial reduction of Cr(VI) and U(VI) by different natural organic matter fractions. Geochem. Cosmochim. Acta 67, 3575–3582. https://doi.org/10.1016/S0016-7037(03)00162-5.

Guria, M.K., Guha, A.K., Bhattacharyya, M., 2014. A green chemical approach for biotransformation of Cr(VI) to Cr(III), utilizing Fusarium sp. MMT1 and

consequent structural alteration of cell morphology. J. Environ. Chem. Eng. 2, 424–433. https://doi.org/10.1016/j.jece.2014.01.016.
Habibul, N., Hu, Y., Wang, Y.K., Chen, W., Yu, H.Q., Sheng, G.P., 2016. Bioelectrochemical chromium(VI) removal in plant-microbial fuel cells. Environ. Sci. Technol. https://doi.org/10.1021/acs.est.5b06376.
Hong, Z., Chen, W., Rong, X., Cai, P., Tan, W., Huang, Q., 2015. Effects of humic acid on adhesion of Bacillus subtilis to phyllosilicates and goethite. Chem. Geol. 416, 19–27. https://doi.org/10.1016/j.chemgeo.2015.10.017.
Hsu, N.H., Wang, S.L., Lin, Y.C., Sheng, G.D., Lee, J.F., 2009. Reduction of Cr(VI) by crop-residue-derived black carbon. Environ. Sci. Technol. 43, 8801–8806. https://doi.org/10.1021/es901872x.
Huang, S.W., Chiang, P.N., Liu, J.C., Hung, J.T., Kuan, W.H., Tzou, Y.M., Wang, S.L., Huang, J.H., Chen, C.C., Wang, M.K., Loeppert, R.H., 2012. Chromate reduction on humic acid derived from a peat soil - exploration of the activated sites on HAs for chromate removal. Chemosphere 87, 587–594. https://doi.org/10.1016/j.chemosphere.2012.01.010.
Huang, X. yue, Ling, L., Zhang, W. xian, 2018. Nanoencapsulation of hexavalent chromium with nanoscale zero-valent iron: high resolution chemical mapping of the passivation layer. J. Environ. Sci. (China) 67, 4–13. https://doi.org/10.1016/j.jes.2018.01.029.
Jaiswal, A., Banerjee, S., Mani, R., Chattopadhyaya, M.C., 2013. Synthesis, characterization and application of goethite mineral as an adsorbent. J. Environ. Chem. Eng. 1, 281–289. https://doi.org/10.1016/j.jece.2013.05.007.
Jiang, L., Zhu, J., Qi, Y., Fu, Q., Hu, H., Huang, Q., 2017. Soil Biology & Biochemistry Increasing molecular structural complexity and decreasing nitrogen availability depress the mineralization of organic matter in subtropical forest soils. Soil Biol. Biochem. 108, 91–100. https://doi.org/10.1016/j.soilbio.2017.01.028.
Jiang, W., Cai, Q., Xu, W., Yang, M., Cai, Y., Dionysiou, D.D., O'Shea, K.E., 2014. Cr(VI) adsorption and reduction by humic acid coated on magnetite. Environ. Sci. Technol. 48, 8078–8085. https://doi.org/10.1021/es405804m.
Johnson, B.B., 1990. Effect of pH, temperature, and concentration on the adsorption of cadmium on goethite. Environ. Sci. Technol. 24, 112–118. https://doi.org/10.1021/es00071a014.
Johnston, C.P., Chrysochoou, M., 2016. Mechanisms of chromate, selenate, and sulfate adsorption on Al-substituted ferrihydrite: implications for ferrihydrite surface structure and reactivity. Environ. Sci. Technol. https://doi.org/10.1021/acs.est.5b05529.
Kang, C., Wu, P., Li, Y., Ruan, B., Li, L., Tran, L., Zhu, N., Dang, Z., 2015. Understanding the role of clay minerals in the chromium(VI) bioremoval by Pseudomonas aeruginosa CCTCC AB93066 under growth condition: microscopic, spectroscopic and kinetic analysis. World J. Microbiol. Biotechnol. 31, 1765–1779. https://doi.org/10.1007/s11274-015-1928-9.
Kang, C., Wu, P., Li, Y., Ruan, B., Zhu, N., Dang, Z., 2014. Estimates of heavy metal tolerance and chromium(VI) reducing ability of pseudomonas aeruginosa CCTCC AB93066: chromium(VI) toxicity and environmental parameters optimization. World J. Microbiol. Biotechnol. 30, 2733–2746. https://doi.org/10.1007/s11274-014-1697-x.
Khattar, J.I.S., Parveen, S., Singh, Y., Singh, D.P., Gulati, A., 2015. Intracellular uptake and reduction of hexavalent chromium by the cyanobacterium Synechocystis sp. PUPCCC 62. J. Appl. Phycol. https://doi.org/10.1007/s10811-014-0374-7.
Kumari, D., Pan, X., Zhang, D., Zhao, C., Al-Misned, F.A., Mortuza, M.G., 2015. Bioreduction of hexavalent chromium from soil column leachate by Pseudomonas stutzeri. Ann. Finance 19, 249–258. https://doi.org/10.1080/10889868.2015.1029116.
Kumpiene, J., Lagerkvist, A., Maurice, C., 2008. Stabilization of As, Cr, Cu, Pb and Zn in soil using amendments - a review. Waste Manag. 28, 215–225. https://doi.org/10.1016/j.wasman.2006.12.012.
Kwak, S., Yoo, J.C., Moon, D.H., Baek, K., 2018. Role of clay minerals on reduction of Cr(VI). Geoderma. https://doi.org/10.1016/j.geoderma.2017.10.001.
Li, C., Yi, X., Dang, Z., Yu, H., Zeng, T., Wei, C., Feng, C., 2016. Fate of Fe and Cd upon microbial reduction of Cd-loaded polyferric flocs by Shewanella oneidensis MR-1. Chemosphere 144, 2065–2072. https://doi.org/10.1016/j.chemosphere.2015.10.095.
Li, Y., Low, G.K.C., Scott, J.A., Amal, R., 2009. The role of iron in hexavalent chromium reduction by municipal landfill leachate. J. Hazard Mater. 161, 657–662. https://doi.org/10.1016/j.jhazmat.2008.04.007.
Liu, T., Li, X., Li, F., Han, R., Wu, Y., Yuan, X., Wang, Y., 2016. In situ spectral kinetics of Cr(VI) reduction by c-type cytochromes in A suspension of living shewanella putrefaciens 200. Sci. Rep. 6, 1–11. https://doi.org/10.1038/srep29592.
Liu, X., Chu, G., Du, Y., Li, J., Si, Y., 2019. The role of electron shuttle enhances Fe(III)-mediated reduction of Cr(VI) by Shewanella oneidensis MR-1. World J. Microbiol. Biotechnol. 35 https://doi.org/10.1007/s11274-019-2634-9, 0.
Lu, J., Fu, F., Zhang, L., Tang, B., 2018. Insight into efficient co-removal of Se(IV) and Cr(VI) by magnetic mesoporous carbon microspheres: performance and mechanism. Chem. Eng. J. 346, 590–599. https://doi.org/10.1016/j.cej.2018.04.077.
Luan, F., Liu, Y., Griffin, A.M., Gorski, C.A., Burgos, W.D., 2015. Iron(III)-bearing clay minerals enhance bioreduction of nitrobenzene by shewanella putrefaciens CN32. Environ. Sci. Technol. 49, 1418–1426. https://doi.org/10.1021/es504149y.
Meng, Y., Zhao, Z., Burgos, W.D., Li, Y., Zhang, B., Wang, Y., Liu, W., Sun, L., Lin, L., Luan, F., 2018. Iron(III) minerals and anthraquinone-2,6-disulfonate (AQDS) synergistically enhance bioreduction of hexavalent chromium by Shewanella oneidensis MR-1. Sci. Total Environ. 640–641, 591–598. https://doi.org/10.1016/j.scitotenv.2018.05.331.
Myers, C.R., Carstens, B.P., Antholine, W.E., Myers, J.M., 2000. Chromium(VI) reductase activity is associated with the cytoplasmic membrane of anaerobically grown Shewanella putrefaciens MR-1. J. Appl. Microbiol. 88, 98–106. https://doi.org/10.1046/j.1365-2672.2000.00910.x.
Nakayasu, K., Fukushima, M., Sasaki, K., Tanaka, S., Nakamura, H., 1999. Comparative studies of the reduction behavior of chromium(VI) by humic substances and their precursors. Environ. Toxicol. Chem. 18, 1085–1090. https://doi.org/10.1897/1551-5028(1999)018<1085:CSOTRB>2.3.CO2.
Ohta, A., Okai, T., Kagi, H., Tsuno, H., Nomura, M., 2012. Speciation study of Cr(VI/III) reacting with humic substances and determination of local structure of Cr binding humic substances using XAFS spectroscopy. Geochem. J. 46, 409–420. https://doi.org/10.2343/geochemj.2.0222.
Ouyang, K., Walker, S.L., Yu, X.Y., Gao, C.H., Huang, Q., Cai, P., 2018. Metabolism, survival, and gene expression of: Pseudomonas putida to hematite nanoparticles mediated by surface-bound humic acid. Environ. Sci. Nano. https://doi.org/10.1039/c7en01039g.
Panagiotakis, I., Dermatas, D., Vatseris, C., Chrysochoou, M., Papassiopi, N., Xenidis, A., Vaxevanidou, K., 2015. Forensic investigation of a chromium(VI) groundwater plume in Thiva, Greece. J. Hazard Mater. 281, 27–34. https://doi.org/10.1016/j.jhazmat.2014.09.048.
Parthasarathy, G., Choudary, B.M., Sreedhar, B., Kunwar, A.C., 2007. Environmental mineralogy: spectroscopic studies on ferrous saponite and the reduction of hexavalent chromium. Nat. Hazards 40, 647–655. https://doi.org/10.1007/s11069-006-9015-z.
Roden, E.E., Kappler, A., Bauer, I., Jiang, J., Paul, A., Stoesser, R., Konishi, H., Xu, H., 2010. Extracellular electron transfer through microbial reduction of solid-phase humic substances. Nat. Geosci. 3, 417–421. https://doi.org/10.1038/ngeo870.
Rong, X., Chen, W., Huang, Q., Cai, P., Liang, W., 2010. Pseudomonas putida adhesion to goethite: studied by equilibrium adsorption, SEM, FTIR and ITC. Colloids Surfaces B Biointerfaces. https://doi.org/10.1016/j.colsurfb.2010.05.037.
Sarkar, B., Naidu, R., Krishnamurti, G.S.R., Megharaj, M., 2013. Manganese(II)-catalyzed and clay-minerals-mediated reduction of chromium(VI) by citrate. Environ. Sci. Technol. 47, 13629–13636. https://doi.org/10.1021/es401568k.
Sathishkumar, K., Murugan, K., Benelli, G., Higuchi, A., Rajasekar, A., 2017. Bioreduction of hexavalent chromium by Pseudomonas stutzeri L1 and Acinetobacter baumannii L2. Ann. Microbiol. 67, 91–98. https://doi.org/10.1007/s13213-016-1240-4.
Scaglia, B., Tambone, F., Adani, F., 2013. Cr(VI) reduction capability of humic acid extracted from the organic component of municipal solid waste. J. Environ. Sci. (China) 25, 487–494. https://doi.org/10.1016/S1001-0742(12)60078-3.
Schwertmann, U., Cornell, R.M., 1992. Iron Oxides in the Laboratory. Preparation and Characterization. Von U. Schwertmann und R. M. Cornell. VCH Verlagsgesellschaft, Weinheim/VCH Publishers, New York. https://doi.org/10.1002/ange.19921041155, 3-527-26991-6/0-89573-858-9, 1991. XIV, 137 S., geb. DM 118.00, Angewandte Chemie.
Shi, L., Squier, T.C., Zachara, J.M., Fredrickson, J.K., 2007. Respiration of metal (hydr) oxides by Shewanella and Geobacter: a key role for multihaem c-type cytochromes. Mol. Microbiol. 65, 12–20. https://doi.org/10.1111/j.1365-2958.2007.05783.x.
Stern, N., Mejia, J., He, S., Yang, Y., Ginder-Vogel, M., Roden, E.E., 2018. Dual role of humic substances as electron donor and shuttle for dissimilatory iron reduction. Environ. Sci. Technol. 52, 5691–5699. https://doi.org/10.1021/acs.est.7b06574.
Stone, J.J., Senko, J.M., Roden, E.E., Kemner, K.M., Burgos, W.D., Kelly, S.D., Dempsey, B.A., 2007. Soil humic acid decreases biological uranium(VI) reduction by shewanella putrefaciens CN32. Environ. Eng. Sci. 24, 755–761. https://doi.org/10.1089/ees.2006.0009.
Swift, R., 1996. Chemical methods. Part 3. In: Sparks, D.E. (Ed.), Methods of Soil Analysis.
Tabatabai, M.A., Sparks, D.L., Senesi, N., Loffredo, E., 2005. Metal Ion Complexation by Soil Humic Substances. https://doi.org/10.2136/sssabookser8.c12.
Tian, X., Wang, W., Tian, N., Zhou, C., Yang, C., Komarneni, S., 2016. Cr(VI) reduction and immobilization by novel carbonaceous modified magnetic Fe3O4/halloysite nanohybrid. J. Hazard Mater. 309, 151–156. https://doi.org/10.1016/j.jhazmat.2016.01.081.
Tribe, L., Kwon, K.D., Trout, C.C., Kubicki, J.D., 2006. Molecular orbital theory study on surface complex structures of glyphosate on goethite: calculation of vibrational frequencies. Environ. Sci. Technol. 40, 3836–3841. https://doi.org/10.1021/es052363a.
Ueshima, M., Ginn, B.R., Haack, E.A., Szymanowski, J.E.S., Fein, J.B., 2008. Cd adsorption onto Pseudomonas putida in the presence and absence of extracellular polymeric substances. Geochem. Cosmochim. Acta 72, 5885–5895. https://doi.org/10.1016/j.gca.2008.09.014.
Us Epa, 1984. Health Assessment Document for Chromium - Final Report.
Venkateswaran, K., Moser, D.P., Dollhopf, M.E., Lies, D.P., Saffarini, D.A., MacGregor, B.J., Ringelberg, D.B., White, D.C., Nishijima, M., Sano, H., Burghardt, J., Stackebrandt, E., Nealson, K.H., 1999. Polyphasic taxonomy of the genus Shewanella and description of Shewanella oneidensis sp. nov. Int. J. Syst. Bacteriol. https://doi.org/10.1099/00207713-49-2-705.
Viamajala, S., Peyton, B.M., Sani, R.K., Apel, W.A., Petersen, J.N., 2004. Toxic effects of chromium (VI) on anaerobic and aerobic growth of shewanella oneidensis MR-1. Biotechnol. Prog. 20, 87–95. https://doi.org/10.1021/bp034131q.
Wang, Y., Sevinc, P.C., Belchik, S.M., Fredrickson, J., Shi, L., Lu, H.P., 2013. Single-cell imaging and spectroscopic analyses of Cr(VI) reduction on the surface of bacterial cells. Langmuir 29, 950–956. https://doi.org/10.1021/la303779y.
Wani, R., Kodam, K.M., Gawai, K.R., Dhakephalkar, P.K., 2007. Chromate reduction by

Burkholderia cepacia MCMB-821, isolated from the pristine habitat of alkaline crater lake. Appl. Microbiol. Biotechnol. https://doi.org/10.1007/s00253-007-0862-7.

Weckhuysen, B.M., Schoonheydt, R.A., 1994. Chemistry and spectroscopy of chromium in zeolites. Stud. Surf. Sci. Catal. 84, 965–972. https://doi.org/10.1016/S0167-2991(08)63630-7.

Zhang, J., Chen, L., Yin, H., Jin, S., Liu, F., Chen, H., 2017. Mechanism study of humic acid functional groups for Cr(VI) retention: two-dimensional FTIR and13C CP/MAS NMR correlation spectroscopic analysis. Environ. Pollut. 225, 86–92. https://doi.org/10.1016/j.envpol.2017.03.047.

Zhang, J., Yin, H., Wang, H., Xu, L., Samuel, B., Chang, J., Liu, F., Chen, H., 2019. Molecular structure-reactivity correlations of humic acid and humin fractions from a typical black soil for hexavalent chromium reduction. Sci. Total Environ. 651, 2975–2984. https://doi.org/10.1016/j.scitotenv.2018.10.165.

Zhang, Y., Zhang, X., Ding, R., Zhang, J., Liu, J., 2011. Determination of the degree of deacetylation of chitosan by potentiometric titration preceded by enzymatic pretreatment. Carbohydr. Polym. https://doi.org/10.1016/j.carbpol.2010.08.058.

Zhao, G., Li, E., Li, J., Liu, Feifei, Liu, Fei, Xu, M., 2019. Goethite hinders azo dye bioreduction by blocking terminal reductive sites on the outer membrane of shewanella decolorationisS12. Front. Microbiol. 10, 1–9. https://doi.org/10.3389/fmicb.2019.01452.

Zhao, G., Li, E., Li, J., Xu, M., Huang, Q., Rong, X., 2018. Effects of interfaces of goethite and humic acid-goethite complex on microbial degradation of methyl parathion. Front. Microbiol. 9, 1–8. https://doi.org/10.3389/fmicb.2018.01748.

Zheng, Z., Li, Y., Zhang, X., Liu, P., Ren, J., Wu, G., Zhang, Y., Chen, Y., Li, X., 2015. A Bacillus subtilis strain can reduce hexavalent chromium to trivalent and an nfrA gene is involved. Int. Biodeterior. Biodegrad. 97, 90–96. https://doi.org/10.1016/j.ibiod.2014.10.017.

Zhenghua, W., Jun, L., Hongyan, G., Xiaorong, W., Chunsheng, Y., 2001. Adsorption isotherms of lanthanum to soil constituents and effects of pH, EDTA and fulvic acid on adsorption of lanthanum onto goethite and humic acid. Chem. Speciat. Bioavailab. 13, 75–81. https://doi.org/10.3184/095422901782775444.

Zhou, S., Xu, J., Yang, G., Zhuang, L., 2014. Methanogenesis affected by the co-occurrence of iron(III) oxides and humic substances. FEMS Microbiol. Ecol. 88, 107–120. https://doi.org/10.1111/1574-6941.12274.

Zhou, X., Liu, D., Bu, H., Deng, L., Liu, H., Yuan, P., Du, P., Song, H., 2018. XRD-based quantitative analysis of clay minerals using reference intensity ratios, mineral intensity factors, Rietveld, and full pattern summation methods: a critical review. Solid Earth Sci 3, 16–29. https://doi.org/10.1016/j.sesci.2017.12.002.